J|A|C|S
ARTICLES
Published on Web 12/09/2006

Mechanism of Electrochemical Charge Transport in Individual Transition Metal Complexes

Tim Albrecht,*,†,|| Adrian Guckian,‡ Alexander M. Kuznetsov,§ Johannes G. Vos,*,‡ and Jens Ulstrup*,†

Contribution from the Department of Chemistry, Nano•DTU, Building 207, Technical University of Denmark, DK-2800 Kongens Lyngby, Denmark, Dublin City University, National Center for Sensor Research, School of Chemical Sciences, Dublin 9, Ireland, and A. N. Frumkin Institute of Physical Chemistry and Electrochemistry, Russian Academy of Sciences, Leniskii Prospekt 31, Bldg. 5, 11907 Moscow, Russia

Received August 26, 2006; E-mail: ta@kemi.dtu.dk; han.vos@dcu.ie; ju@kemi.dtu.dk

Abstract: We used electrochemical scanning tunneling microscopy (STM) and spectroscopy (STS) to elucidate the mechanism of electron transport through individual pyridyl-based Os complexes. Our tunneling data obtained by two-dimensional electrochemical STS and STM imaging lead us to the conclusion that electron transport occurs by thermally activated hopping. The conductance enhancement around the redox potential of the complex, which is reminiscent of switching and transistor characterics in electronics, is reflected both in the STM imaging contrast and directly in the tunneling current. The latter shows a biphasic distance dependence, in line with a two-step electron hopping process. Under conditions where the substrate/molecule electron transfer (ET) step is dominant in determining the overall tunneling current, we determined the conductance of an individual Os complex to be 9 nS ($V_{bias} = 0.1$ V). We use theoretical approaches to connect the single-molecule conductance with electrochemical kinetics data obtained from monolayer experiments. While the latter leave some controversy regarding the degree of electronic coupling, our results suggest that electron transport occurs in the adiabatic limit of strong electronic coupling. Remarkably, and in contrast to established ET theory, the redox-mediated tunneling current remains strongly distance dependent due to the electronic coupling, even in the adiabatic limit. We exploit this feature and apply it to electrochemical single-molecule conductance data. In this way, we attempt to paint a unified picture of electrochemical charge transport at the single-molecule and monolayer levels.

1. Introduction

Charge transport processes in individual molecules and in other nanoscale and mesoscopic structures have been in scientific focus over the past decade.[1−4] In addition to offering new fundamental insight, these efforts have been fueled by expectations regarding the development of electronic devices and circuitry based on ultrasmall structures or even single molecules.[5−8] Such concepts could pave the way toward further device miniaturization, once silicon-based chip technology has reached its physical limits.[4]

Techniques employed to study single-molecule charge transport have included scanning-probe microscopies and nanoscale electrodes fabricated by break-junction techniques, electromigration, and lithography, sometimes including electrodeposition.[9−15] Most studies refer to "ex situ" conditions, i.e., in air or a vacuum, and at cryogenic temperatures.[16−19] Condensed

† Technical University of Denmark.
‡ Dublin City University.
§ Russian Academy of Sciences.
|| Present address: Imperial College London, Chemistry Dept., Bldg. C1, London SW7 2AZ, UK.

(1) McCreery, R. L. *Anal. Chem.* **2006**, *11*, 3490−3497 and references therein.
(2) Tour, J. M. *Molecular Electronics: Commercial Insights, Chemistry, Devices, Architecture, and Programming*; World Scientific: Singapore, 2003.
(3) Aviram, A. *Molecular Electronics II*; Annals of the New York Academy of Sciences; Johns Hopkins University Press: 2003; notice also vols. I and III in the same series.
(4) Waser, R., Ed. *Nanoelectronics and Information Technology - Advanced Electronic Materials and Novel Devices*; Wiley-VCH: 2003.
(5) Avouris, P. *Acc. Chem. Res.* **2002**, *35*, 1026−1034.
(6) Heath, J. R.; Kuekes, P. J.; Snider, G. S.; Williams, R. S. *Science* **1998**, *280*, 1716−1721.
(7) Collier, C. P.; Wong, E. W.; Belohradsky, M.; Raymo, F. M.; Stoddart, J. F.; Kuekes, P. J.; Williams, R. S.; Heath, J. R. *Science* **1999**, *285*, 391−394.
(8) Collier, C. P.; Mattersteig, G.; Wong, E. W.; Luo, Y.; Beverly, K.; Sampaio, J.; Raymo, F. M.; Stoddart, J. F.; Heath, J. R. *Science* **2000**, *289*, 1172−1175.
(9) Salomon, A.; Cahen, D.; Lindsay, S.; Tomfohr, J.; Engelkes, V. B.; Frisbie, C. D. *Adv. Mat.* **2003**, *15*, 1881−1890.
(10) Wold, D. J.; Haag, R.; Rampi, M. A.; Frisbie, C. D. *J. Phys. Chem. B* **2002**, *106*, 2813−2816.
(11) Moth-Poulsen, K.; Patrone, L.; Stuhr-Hansen, N.; Christensen, J. B.; Bourgoin, J. P.; Bjørnholm, Th. *Nano Lett.* **2005**, *5*, 783−785.
(12) Moreland, J.; Ekin, J. W. *J. Appl. Phys.* **1985**, *58*, 3888−3895.
(13) Park, H.; Lim, A. K. L.; Alivisatos, A. P.; Park, J.; McEuen, P. L. *Appl. Phys. Lett.* **1999**, *75*, 301−303.
(14) Li, C. Z.; He, H. X.; Tao, N. J. *Appl. Phys. Lett.* **2000**, *77*, 3995−3997.
(15) Kervennic, Y. V.; Vanmaekelbergh, D.; Kouwenhoven, L. P.; van der Zant, H. S. J. *Appl. Phys. Lett.* **2003**, *83*, 3782−3784.
(16) Liang, W.; Shores, M. P.; Bockrath, M.; Long, J. R.; Park, H. *Nature* **2002**, *417*, 725−729.
(17) Nazin, G. V.; Qiu, X. H.; Ho, W. *Science* **2003**, *302*, 77−81.
(18) Park, J.; Pasupathy, A. N.; Goldsmith, J. I.; Chang, C.; Yaish, Y.; Petta, J. R.; Rinkoski, M.; Sethna, J. P.; Abruna, H. D.; McEuen, P. L.; Ralph, D. C. *Nature* **2002**, *417*, 722−725.

10.1021/ja066213r CCC: $33.50

media, particularly electrochemical environments, where nanogap electrode configurations and electrochemical scanning tunneling microscopy (in situ STM) are prominent, offer additional perspectives. In such configurations, substrate and tip electrodes, equivalent to source and drain electrodes in a transistor, are operated in bipotentiostatic mode; i.e., their electrochemical potentials are independently controlled with respect to a common reference electrode. The latter acts as an electrochemical "gate" and modulates the tunneling current between source and drain (substrate and tip) electrodes.[20−31] In this way, redox-active molecules in the tunneling gap can be brought to display transistor and diode characteristics in the condensed matter environment and *at room temperature*, making them potentially attractive in efforts toward molecular electronics.[32]

Charge-transfer processes in electrochemical systems hold qualitative differences compared to solid-state environments.[33,34] Electronic energy levels in nanoscopic solid-state components are modulated largely by the external circuitry (bias voltage and gate potential). The electronic levels of electrochemical molecular scale components, say redox molecules, are in general also strongly coupled to the nuclear environmental motion, extending to both local molecular modes and the aqueous or ionic liquid environment.[25,33] As a result, the equilibrium electronic energies of the vacant (oxidized) and occupied (reduced) levels are widely different, separated by twice the total nuclear reorganization free energy, λ, which accompanies the charge-transfer process. In addition, electronic−vibrational coupling leads to broadening of the levels by a similar range, say $\lambda \approx 0.2-0.5$ eV, i.e., significantly larger than thermal broadening under ambient conditions (∼26 meV at 298 K). Environmental configurational fluctuational effects on the electronic energy levels are therefore other crucial features of molecular scale condensed matter electronic processes. In a sense this leads to a "band structure" for the redox species and a Fermi level where the vibrational densities of states (DOS) functions of the oxidized and reduced states coincide, DOS(ox) = DOS(red).[35]

The origin of the bands is, however, quite different compared to metal or semiconductor structures, and the concentrations of reduced and oxidized species and the DOS functions therefore depend on the applied potential according to the Nernst equation.

In electron (hole) hopping via molecular redox centers, the current depends on both the density of available states at a given energy ϵ, DOS$(\epsilon)_i$, and the individual interfacial electron transfer (ET) rate constants, $k_{ET,i}$. Charge transfer is in general thermally activated and the molecular "standard Fermi level" ϵ_F° of prime importance. ϵ_F° refers to the equilibrium redox potential of the molecule, E°, where the concentrations of oxidized and reduced molecules are the same. Both the product DOS(ox)·DOS(red) and the product of the individual hopping rate constants, $k_{ET,i}$, are here maximum. This general observation suggests that electron hopping is most efficient around the equilibrium potential of a redox species. Our recent experimental work has supported this hypothesis.[23,25] It should also be noted that the local potential at the redox site can be modulated with both the tip/substrate bias voltage and the overpotential (gate potential).

Thermally induced molecular "gating" of the tunneling process through nonredox or redox molecules has emerged as still another feature of room-temperature molecular scale conductivity. The notion "gating" here implies that configurational fluctuations in certain nuclear modes lead to a nonequilibrium configuration optimal for ET followed by relaxation back to the original equilibrium configuration. Such charge-transfer processes are accompanied by a substantial apparent activation energy, which is, however, conceptually different from nuclear reorganization in the actual sense of ET theory. Allara et al. and Haiss et al. studied configurationally gated tunneling for alkyldithiols and determined the apparent activation energy in the gating mode.[36,37] This is another example where room-temperature molecular tunneling clearly goes beyond mere electronic conductivity and also involves more composite charge-transfer features.

In this report we address fundamentals of condensed matter room-temperature single-redox-molecule electronic charge transport by a combined experimental and theoretical effort. We investigate in some detail interfacial ET via the redox level of a "strategically" chosen Os complex, $[Os(bpy)_2(p0p)Cl]$ ("Osp0p"; bpy = 2,2′-bipyridyl; p0p = 4,4′-bipyridyl), immobilized on a single-crystal Pt(111) surface by electrochemical techniques and electrochemical STM. Such transition metal complexes are robust, highly stable in the two oxidation states, Os(II) and Os(III), and likely to represent a whole class of redox switchable molecules for molecular electronics.[38] Resting on previous results for this and other transition metal complexes, we determine the conductivity of a single molecule. We further estimate the electronic transmission coefficient between the redox molecule and the Pt(111) substrate electrode at the single-molecule level as one of the most crucial interfacial ET parameters. We finally elaborate new theoretical schemes for condensed matter room-temperature three-level ET, allowing us to estimate the number of electrons coherently transmitted

(19) Kubatkin, S.; Danilov, A.; Hjort, M.; Cornil, J.; Brédas, J. L.; Stuhr-Hansen, N.; Hedegard, P.; Bjørnholm, Th. *Nature* **2003**, *425*, 698−701.
(20) Tao, N. J. *Phys. Rev. Lett.* **1996**, *76*, 4066−69.
(21) Xiao, X.; Nagahara, L. A.; Rawlett, A. M.; Tao, N. J. *J. Am. Chem. Soc.* **2005**, *127*, 9235−9240.
(22) Chen, F.; He, J.; Nuckolls, C.; Roberts, T.; Klare, J. E.; Lindsay, S. *Nano. Lett.* **2005**, *5*, 503−506.
(23) Albrecht, T.; Guckian, A.; Ulstrup, J.; Vos, J. G. *Nano Lett.* **2005**, *5*, 1451−1455.
(24) Albrecht, T.; Moth-Poulsen, K.; Christensen, J. B.; Guckian, A.; Bjørnholm, Th.; Vos, J. G.; Ulstrup, J. *Faraday Discuss.* **2006**, *131*, 265−279.
(25) Albrecht, T.; Moth-Poulsen, K. Christensen, J. B.; Hjelm, J.; Bjørnholm, Th.; Ulstrup, J. *J. Am. Chem. Soc.* **2006**, *128*, 6574−6575.
(26) Chi, Q. J.; Farver, O.; Ulstrup, *J. Proc. Nat. Acad. Sci. U.S.A.* **2005**, *102*, 16203−16208.
(27) Yokota, Y.; Miyazaki, A.; Fukui, K.; Enoki, T.; Hara, M. *J. Phys. Chem. B* **2005**, *109*, 23779−23782.
(28) Holmlin, R. E.; Ismagilov, R. F.; Haag, R.; Mujica, V.; Ratner, M. A.; Rampi, M. A.; Whitesides, G. M. *Angew. Chem., Int. Ed.* **2001**, *40*, 2316−2320.
(29) Tran, E.; Rampi, M. A.; Whitesides, G. M. *Angew. Chem., Int. Ed.* **2004**, *43*, 3835−3839.
(30) Alessandrini, A.; Salerno, M.; Frabboni, S.; Facci, P. *Appl. Phys. Lett.* **2005**, *86*, 133902
(31) Li, Z.; Han, B.; Meszaros, G.; Pobelov, I.; Wandlowski, T.; Blaszcyk, A.; Mayor, M. *Faraday Discuss.* **2006**, *131*, 121−143.
(32) Zhang, J.; Chi, Q.; Kuznetsov, A. M.; Hansen, A. G.; Wackerbarth, H.; Christensen, H. E. M.; Andersen, J. E. T.; Ulstrup, J. *J. Phys. Chem. B* **2002**, *106*, 1131−1152.
(33) Kuznetsov, A. M.; Ulstrup, J. *Electron transfer in chemical and biology: An introduction to the theory*; Wiley Series in Theoretical Chemistry; John Wiley & Sons Ltd.: 1999.
(34) Sato, N. *Electrochemistry at Metal and Semiconductor Electrodes*; Elsevier: 1998.
(35) Gerischer, H. *Z. Phys. Chem.* **1960**, *26*, 223−247. *Z. Phys. Chem.* **1960**, *26*, 325−338. *Z. Phys. Chem.* **1961**, *27*, 48−79.
(36) Selzer, Y.; Cabassi, M. A.; Mayer, T. S.; Allara, D. L. *J. Am. Chem. Soc.* **2004**, *126*, 4052−4053.
(37) Haiss, W.; van Zalinge, H.; Bethell, D.; Ulstrup, J.; Schiffrin, D. J.; Nichols, R. J. *Faraday Discuss.* **2006**, *131*, 253−264.
(38) Low, P. J. *Dalton Trans.* **2005**, *17*, 2821−2824.

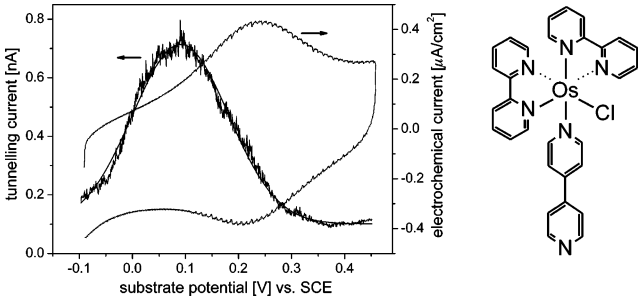

Figure 1. CV (right ordinate) and STS (left ordinate, including Gaussian fit) of Osp0p on Pt(111). 0.1 M aqueous $NaClO_4$; $V_{bias} = (E_t - E_s) = +0.1$ V; $I^{\circ}_{set} = 0.1$ nA. Right: Molecular structure (schematic).

in a single charge-transfer event as a novel feature in three-level adiabatic interfacial ET.

2. Experimental Section

$[Os(bpy)_2(p0p)Cl](PF_6)$ was synthesized and Pt(111) electrodes were prepared as previously.[24] Other reagents were of highest available grade. Millipore water was used throughout (18.2 MΩ·cm). $[Os(bpy)_2(p0p)Cl]^{+/2+}$, Figure 1, was immobilized on Pt(111) by soaking the electrodes overnight in 10−50 μM water/dimethylformamide solutions (H_2O/DMF = 2:1 (m/m)), followed by rinsing with Millipore water and 0.1 M aqueous $NaClO_4$.

An electrochemical Autolab system with SCANGEN/ADC750 modules controlled by the GPES software (Ecochemie, Netherlands) was used. Electrochemical (glass) cells were custom-made. All cyclic voltammograms were recorded in linear scan mode. A freshly prepared reversible hydrogen electrode (RHE) and a Pt wire served as the reference and counter electrode, respectively. The reference electrode was calibrated against a saturated calomel electrode (SCE) after each experiment. Electrodes (area: ∼0.03 cm^2) were employed in the hanging-meniscus configuration. Prior to each experiment, the electrochemical cell was deoxygenated by purified Ar (Chrompack O_2 filter), and a steady flow of Ar was maintained during operation. Aqueous 0.1 M $NaClO_4$ was used as the electrolyte.

A PicoSPM instrument (Molecular Imaging Co., USA) with a bipotentiostat for independent control of substrate and tip potential was used in constant-current mode for STM imaging. The custom-made three-electrode Teflon cell was equipped with Pt wires as counter and reference electrodes, the latter calibrated against a SCE electrode after each experiment. The Pt(111) substrate (Mateck, Germany) was flame-annealed in a hydrogen flame, cooled in a H_2 flow until the red glow had disappeared, and quenched in H_2O (electroactive area: 0.5 cm^2). Electrolytes were as those in the electrochemical experiments.

For experiments with the feedback loop switched off, i.e., for $I_t(E_s)$ spectroscopy at constant bias voltage, the tip was approached to a certain setpoint current inside the tunneling range (I°_{set}).The initial potential, $E_{s,i}$, was set suitably remote from E°. The feedback loop was then switched off, and the substrate potential E_s cycled once in a potential range wide enough to pass the equilibrium redox potential of the complex with both E_s and the tip potential E_t. The bias voltage between tip and substrate, $V_{bias} = E_t - E_s$, was kept constant. $E_{s,i}$ thus equals the final potential of the cycle, $E_{s,f}$. The difference in tunneling current before and after a scan was used as an indicator for lateral and/or vertical drift and to assess the quality of an $I_t(E_s)$ scan. It was concluded from STM imaging that lateral drift usually amounted to about one molecular diameter for sweep durations of 5 s.

3. Results and Discussion

3.1. Tunneling Spectroscopy and in Situ STM of Osp0p. We have previously reported redox-mediated tunneling current enhancement through inorganic transition metal complexes in

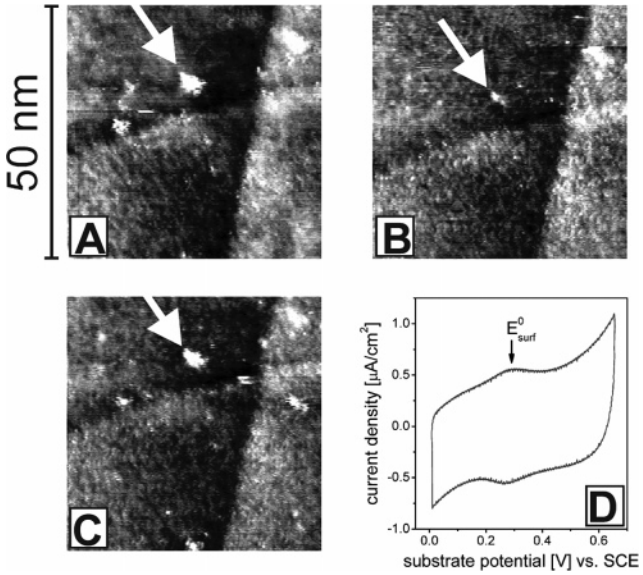

Figure 2. STM imaging of Osp0p on Pt(111) in 0.1 M $NaClO_4$. E°_{surf} (Osp0p) = 0.24 V. (A and C) $E_s = 0.34$ V; (B) $E_s = 0.59$ V ($I_{set} = 0.1$ nA, $V_{bias} = -0.2$ V in all cases; p0p as lateral) spacer; (D) cyclic voltammogram of Osp0p/p0p on Pt(111); 0.1 M $NaClO_4$, $\nu = 0.1$ V/s (all potentials vs SCE).

electrochemical STM. As noted, the reference electrode is here equivalent to an electrochemical transistor gate.

A typical monolayer cyclic voltammogram (CV) of Osp0p is shown in Figure 1, right ordinate, indicating the position of the (surface) redox potential $E^{\circ}_{surf} = +0.24$ V vs SCE. For a detailed discussion of the electrochemical properties of Osp0p and its structural homologues $[Os(bpy)_2(p2p)Cl]^{+/2+}$ ("Osp2p") and $[Os(bpy)_2(p3p)Cl]^{+/2+}$ ("Osp3p"), we refer to previous work (p2p: 4,4′-bipyridyl-1,2-bis(4-pyridyl)ethane); p3p: 4,4′-trimethylenedipyridine).[24,39−46] The corresponding tunneling signal is measured in electrochemical STM by sweeping the substrate potential E_s at a constant tunneling distance and V_{bias} (constant height mode), Figure 1 left ordinate. A significant enhancement of the tunneling current could be detected with a distinct maximum close to E°_{surf}. Its exact position depends on the local potential at the redox site and, thus, on the applied tip/substrate bias $V_{bias} = E_t - E_s$; cf. below.[23]

STM imaging in constant-current mode around the redox potential of the complex at constant V_{bias} also shows the observed conductivity enhancement, Figure 2. The conductivity is then reflected in the apparent height of a surface feature or its STM contrast. This observation qualitatively supports our interpretation of the STS data as a tunneling process involving only a few or even single molecules.

For the experiment shown in Figure 2, Osp0p was coadsorbed with the electrochemically inactive "spacer" molecule, 4,4′-bipyridine ("p0p"), so that the average distance between different Os complexes on the surface is large and the p0p layer can be

(39) Forster, R. J.; Faulkner, L. R. *J. Am. Chem. Soc.* **1994**, *116*, 5454−5462.
(40) Forster, R. J.; Figgemeier, E.; Loughman, P.; Lees, A.; Hjelm, J.; Vos, J. G. *Langmuir.* **2000**, *16*, 7871−7875.
(41) Forster, R. J.; Loughman, P.; Keyes, T. E. *J. Am. Chem. Soc.* **2000**, *122*, 11948−11955.
(42) Forster, R. J.; O'Kelly, J. P. *J. Electrochem. Soc.* **2001**, *148*, E31−E37.
(43) Forster, R. J. *Inorg. Chem.* **1996**, *35*, 3394−3403.
(44) Forster, R. J.; Faulkner, L. R. *Anal. Chem.* **1995**, *67*, 1232.
(45) Hudson, J. E.; Abruna, H. D. *J. Phys. Chem.* **1996**, *100*, 1036−1042.
(46) Inose, Y.; Moniwa, S.; Aramata, A.; Yamagishi, A.; Naing, K. *Chem. Commun.* **1997**, *1*, 111−112.

used as a reference molecule for apparent height measurements. In Figure 2A, E°_{surf} lies within the potential window of tip and substrate potential and thus in the potential region of the tunneling current peak, Figure 1. The surface structure at the potential indicated by the white arrow shows a large apparent height, 7 ± 0.5 Å relative to the p0p layer (average of eight images), corresponding to high local conductivity. The same structure is imaged in Figure 2B, but with E_t and E_s far from E°_{surf} (same V_{bias}). The structure is now significantly smaller with an apparent height of 4.5 ± 0.5 Å indicating a lower local conductivity (average of four images). When the potentials of Figure 2A were restored, Figure 2C, the surface structure reappeared with the same apparent height of 7 Å, illustrating the reversibility of the effect. Experimental parameters other than substrate and tip potentials, such as the settings of the STM feedback loop, remained unchanged. We hesitate to analyze the apparent height change in more quantitative terms, for example, as done by Weiss et al. or Bjørnholm et al. for organic molecules in ex situ STM configurations.[11,47,48] In the present case, the charge-transfer process is quite complex in nature, as illustrated by the strong substrate potential dependence of the effective electronic decay factor β for Os(p0p) layers on Pt(111) substrates (0.1 M aqueous $NaClO_4$).[24] Instead, we will use STS data for a quantitative assessment, which directly yield the tunneling current as a function of bias voltage and overpotential; see below.

It is difficult to assess the number of molecules represented by the structure highlighted in Figure 2. Assuming a statistical distribution, Osp0p should be sufficiently diluted on the surface to be isolated as single molecules in a matrix of p0p. The features in Figure 2, however, appear much wider than the molecular geometries of Osp0p, and their apparent size depends strongly on the potential settings. In images preceding Figure 2A, several structures of the same size were present. Their number decreased with time, possibly due to tip interference or slow desorption, but they always disappeared as a whole, not as fractions, Figure S1 in the Supporting Information. These observations suggest that the structure indeed represents a single molecule. The increased dimensions can then be understood as the result of tip/molecule convolution.

3.2. Molecular Tunneling Mechanisms of Osp0p. We address next the molecular ET mechanism in more detail. We have shown previously that electron transport in the STM tunneling gap occurs via two-step electron hopping, i.e., two sequential ET steps with full vibrational relaxation in between, at least when the bias voltage V_{bias} is smaller than the environmental nuclear reorganization energy λ (say $V_{bias} \leq 0.3$ V).[23,24,32] In accordance with this model, a tunneling current peak feature was detected close to the redox potential of $[Os(bpy)_2(p0p)Cl]^{+/2+}$. Its exact position depends on V_{bias} and coincides with E°_{surf} for $V_{bias} \rightarrow 0$ V.[32] This is in contrast to single-state tunneling, for example, where the maximum tunneling enhancement is at $E^{\circ}_{surf} \pm \lambda$, i.e., shifted from E°_{surf} by the reorganization energy λ.[49,50] λ generally includes both intramolecular and environmental contributions, λ_{mol} and λ_{sol}, respectively. The latter often dominates in electrochemical and solution-based electron exchange processes, but its importance is less obvious in the STM tunneling gap where the solvent is (partly) displaced and the environmental reorganization energy λ_{sol} is presumably lower due to the close proximity of the STM tip. This also implies that λ_{sol} could depend on the tip/substrate distance, as the latter affects both the amount of solvent present and the electric field in the tunneling gap. In extreme cases, λ_{sol} may become small compared to λ_{mol} which then dominates the total reorganization energy λ.

λ_{mol} reflects changes in the molecular geometry between the oxidized and reduced state. Crystallographic data for Os and Ru complexes similar to $[Os(bpy)_2(p0p)Cl]^{+/2+}$, in both oxidation states ((II) and (III)), suggest that λ_{mol} is small in the present case.[51−53] λ_{mol} is also only indirectly affected by the tip, for example due to the effect of local electric fields on the molecular geometry.

Major alterations in the molecular or electronic structure on immobilization or due to the presence of the STM tip can, further, be ruled out as the molecular properties of the complex, such as the surface redox potential E°_{surf}, remain almost the same as those in solution. Immobilized Osp0p exhibits a redox potential of +0.24 V vs SCE in 0.1 M $NaClO_4$, Figure 1, while a structurally closely related complex, $[Os(bpy)_2(py)Cl]^{+/2+}$, has a solution redox potential of $E^{\circ} = +0.24$ V (py: pyridine).[54] This is supported by resonance Raman (RR) and surface-enhanced (resonance) Raman spectral data of pyridine-based Os and Ru complexes in solution and on rough Au or Ag surfaces. Vibrational frequencies are shifted only by a few wavenumbers, showing that the molecular structure is retained.[55−57]

Forster et al. determined both the interfacial electrochemical ET rate constants, $k_{ET,ec}$, and the total electrochemical reorganization energy λ of $[Os(bpy)_2(p2p)Cl]^{+/2+}$ ("Osp2p") and $[Os(bpy)_2(p3p)Cl]^{+/2+}$ ("Osp3p"). The latter was found to be 0.3−0.4 eV for monolayers immobilized on polycrystalline Pt electrode surfaces (chloroform).[39,58] Bearing in mind both that chloroform is notably less polar than water and that λ_{sol} in the tunneling gap is equal to or smaller than this value, the latter should constitute an upper limit of λ in the electrochemical STM configuration. To the best of our knowledge, no experimental kinetic data for immobilized Osp0p in aqueous 0.1 M $NaClO_4$ are available. There are, however, extensive high-quality data for Osp0p in other solvents, as well as for Osp2p and Osp3p in various organic and aqueous environments (all on polycrystalline Pt).[24,39−45,58] We therefore use the distance- and solvent-dependence of $k_{ET,ec}$ independently, in order to obtain an estimate for $k_{ET,ec}$(Osp0p) in aqueous 0.1 M $NaClO_4$. Both approaches yield the same order of magnitude, namely $k_{ET,ec}$-

(47) Bumm, L. A.; Arnold, J. J.; Cygan, M. T.; Dunbar, T. D.; Burgin, T. P.; Jones, L., II; Allara, D. L.; Tour, J. M.; Weiss, P. S. *Science* **1996**, *271*, 1705−1707.
(48) Bumm, L. A.; Arnold, J. J.; Dunbar, T. D.; Allara, D. L.; Weiss, P. S. *J. Phys. Chem. B* **1999**, *103*, 8122−8127.
(49) Kuznetsov, A. M.; Ulstrup, J. *J. Phys. Chem. A* **2000**, *104*, 11531−11540.
(50) Schmickler, W.; Widrig, C. *J. Electroanal. Chem.* **1992**, *336*, 213−221. Schmickler, W. *Surf. Sci.* **1993**, *295*, 43−56. Kuznetsov, A. M.; Schmickler W. *Chem. Phys.* **2002**, *282*, 371−377.
(51) Goodwin, H. A.; Kepert, D. L.; Patrick, J. M.; Skelton, B. W.; White, A. H. *Aust. J. Chem.* **1984**, *37*, 1817−1824.
(52) Fergusson, J. E.; Robinson, W. T.; Love, J. L. *Inorg. Chem.* **1972**, *11*, 1662−1666.
(53) Ryabov, A. D.; Roznyatovskaya, N. V.; Suwinska, K.; Revenco, M.; Ershov, A. Y. *J. Biol. Inorg. Chem.* **2003**, *8*, 815−822.
(54) Buckingham, D. A.; Sargeson, A. M. In *Chelating agents and metal chelate*; Dwyer and Meller, Eds.; Academic Press: 1964; Chapter 6.
(55) Taylor, A. P.; Crayston, J. A.; Dines, T. J. *J. Chem. Soc., Faraday Trans.* **1997**, *93*, 1803−1812.
(56) Tognalli, N.; Fainstain, A.; Bonazzola, C.; Calvo, E. *J. Chem. Phys.* **2004**, *120*, 1905−1911.
(57) Tognalli, N.; Fainstain, A.; Bonazzola, C.; Calvo, E.; Pietrasanta, L.; Campoy-Quiles, M.; Etchegoin, P. *J. Chem. Phys.* **2005**, *123*, 044707.
(58) Forster, R. J.; Faulkner, L. R. *J. Am. Chem. Soc.* **1994**, *116*, 5444−5452.

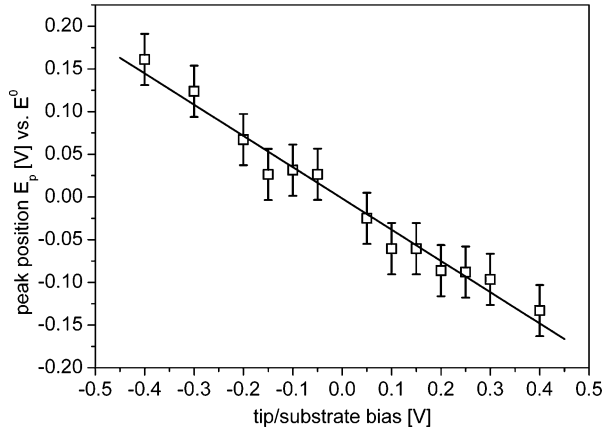

Figure 3. Tunneling current peak position relative to $E°$ as a function of $V_{bias} = E_t - E_s$. Each point is an average of at least 10 scans. Linear fit yields a slope of -0.37 ± 0.02 and an intercept of -0.002 V $\pm$ 0.03 V.

(Osp0p) = 10^7-10^8 s^{-1}. The procedure is described on p S2 in the Supporting Information.

The molecular structural parameters hold a first clue to the tunneling mechanism as a coherent or sequential two-state electron transfer. The strong tunneling current enhancement close to $E°_{surf}$ is detected for Osp0p, but also other Os complexes.[23−25,59] Further, no peak features appeared down to substrate potentials of -0.55 V relative to $E°_{surf}$. Within a single-state tunneling model, this can only be rationalized if λ is larger than, say, 0.6 eV ($V_{bias} = -0.1$ V).[49,50] This is much larger than λ determined from electrochemistry which was considered an upper limit in the present case. Coherent or sequential, two-state electron hopping, and not single-state tunneling ET, therefore emerges clearly as the dominating mechanism.

This is strongly supported by data shown in Figure 3. The tunneling current peak position depends linearly on V_{bias} with an intercept of 0 $\pm$ 0.03 V and a slope of -0.37, in full accordance with the two-state mechanism.[32]

3.3. Single-Molecule Conductivity of Osp0p. The number of molecules contributing to the tunneling process is, finally, a central issue. This number can be assessed in the following way. If a small number of molecules is "wired" in parallel, i.e., if mutual interactions are unimportant, their conductivities are additive to a first approximation. When the STM tip drifts over a monolayer of Osp0p, one expects that, depending on its exact position over the surface, different numbers of molecules contribute to the tunneling process. Due to the strong distance dependence of the tunneling effect, this number is presumably small, say between one and three or four. We have therefore analyzed the abundance distribution of tunneling current peak intensities, as shown in Figure 4 (Pt(111), 0.1 M $NaClO_4$, $V_{bias} = -0.1$ V, $I°_{set} = 0.05$ nA).

It appears that the tunneling current peak intensities are not randomly distributed but grouped around equally spaced tunneling current values. In our interpretation above, these represent different numbers of molecules participating in the tunneling process. The inset in Figure 4 shows a plot of the maximum peak abundances vs the peak number. The intercept is close to zero, indicating that the first peak indeed corresponds to a single

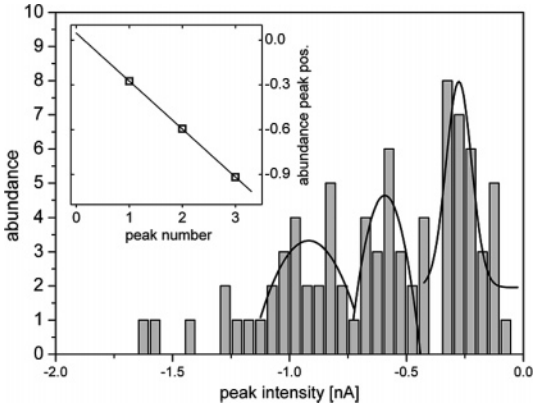

Figure 4. Abundance of tunneling current peak intensities, cf. Figure 1; $V_{bias} = -0.1$ V, $I°_{set} = 0.05$ nA. Inset: Peak position vs peak number, linear fit: slope = -0.32 nA/peak, intercept = 0.05 nA.

molecule. The slope gives a tunneling current/molecule of 0.32 nA/molecule. The $I_t(\eta)$ curve shown in Figure 1 would therefore represent specifically two molecules in the charge-transfer process.

3.4. Tunneling Peak Current Intensity and Distance Variation. The dependence of the peak intensity on the initial setpoint current $I°_{set}$, i.e. tip/substrate distance, holds other clues to the tunneling mechanism. $I°_{set}$ is the initial setpoint tunneling current where the feedback loop was switched off and the tunneling distance no longer (actively) changed.

The absolute tip/substrate distance is not known at given setpoint currents, but an increase in $I°_{set}$ corresponds to a relative decrease in tip/substrate distance. As the substrate/molecule distance is given by the molecular geometry and remains fixed, essentially the tip/molecule distance varies by varying $I°_{set}$. We refer the data to the following transparent formalism and confine the discussion to the adiabatic limit of strong interaction between the molecule and the enclosing electrodes (see, however, below). The tunneling current can be expressed by eq 1.[32]

$$i_{tun} = 2\, e\, n_{el}\, \frac{k_{sm}\, k_{mt}}{k_{sm} + k_{mt}} \qquad (1)$$

where n_{el} is the number of electrons transferred within a characteristic nuclear relaxation time τ_{nucl}, e, the electronic charge, and k_{mt} and k_{sm}, the rate constants for ET from tip to molecule and from molecule to substrate, respectively ($V_{bias} < 0$). The rate constants in the adiabatic limit are

$$k_{sm} = \frac{\omega_{eff}}{2\pi} \exp\left[-\frac{(\lambda - e\,\xi\,\eta - e\,\gamma\,V_{bias})^2}{4\;\lambda\,k_B\,T} \right] \qquad (2)$$

with an analogous expression for k_{mt}. ω_{eff} is the effective vibrational frequency of all the local and environmental nuclear modes reorganized in the electronic transitions and η the overpotential, k_B is Boltzmann's constant, and T is the temperature. The parameters ξ and γ represent the fraction of substrate potential and bias voltage drops, respectively, at the redox site. Rate constant forms such as these are broadly known from the theory of interfacial electrochemical ET.[33]

n_{el} in eq 1 is given by the redox level broadening caused by the electronic interactions with the enclosing substrate and tip electrodes. The broadening can be recast in terms of the apparent

(59) Albrecht, T.; Guckian, A.; Ulstrup, J.; Vos, J. G. *IEEE Trans. Nanotechnol.* **2005**, *4*, 430−434.

electronic transmission coefficients, κ_i, and the metallic substrate and tip electronic densities, ρ, giving:

$$n_{el} = \frac{e\,V_{bias}}{\Delta\epsilon} = e\,V_{bias}\left(\frac{1}{\rho\,\kappa_{sm}} + \frac{1}{\rho\,\kappa_{mt}}\right)^{-1} \qquad (3)$$

$\Delta\epsilon$ represents the energy range in the window between the substrate and tip Fermi levels through which the temporarily occupied redox level relaxes before the electron is transmitted. $\Delta\epsilon$ is small, i.e., $\Delta\epsilon \ll k_BT$ in the adiabatic limit of strong electronic coupling and broadening, giving $n_{el} \gg 1$. It is large, $\Delta\epsilon \gg k_BT$, in the strongly diabatic limit of weak coupling, where $eV/\Delta\epsilon$ should be replaced by 1. Details are given elsewhere.[32,49] The subscripts of κ refer to the substrate/molecule (sm) and molecule/tip (mt) ET step, eq 3. For the sake of simplicity ρ is taken to be the same for the substrate and tip. κ_i (i = sm, mt) is given by the following form also known from the theory of electrochemical ET.[33]

$$\kappa_i = [T(_{\epsilon A}\epsilon;\eta)]_i^2 \sqrt{\frac{4\pi^3}{\lambda k_B T \hbar^2\,\omega_{eff,i}^2}} \qquad (4)$$

where $T_{\epsilon A}(\epsilon;\,\eta)$ is the electronic coupling between the molecular redox level and a given metallic electronic level at the energy ϵ approximately at the Fermi level ϵ_F. $\hbar$ is Planck's constant divided by 2π.

In an electronically highly asymmetric junction, say $\kappa_{mt} >> \kappa_{sm}$, eq 1 can be simplified to

$$I_{tun}^{peak} = en_{el}\,k_{sm}^{peak} = e^2V_{bias}\rho\kappa_{sm}k_{sm}^{peak} \qquad (5)$$

with

$$n_{el} = eV_{bias}\rho\kappa_{sm}$$

Equations 1−4 prompt some observations. The dependence of the two-step tunneling current on the effective frequency, ω_{eff}, vanishes due to cancellation of this factor from eqs 1, 2, and 4. The appearance of an apparent electronic transmission coefficient in the tunneling current *also* in the adiabatic limit is, second, notable as the electronic transmission coefficients of the individual ET steps approach unity in this limit. The κ_i-form in eq 4 is further not confined to $\rho\kappa_i k_BT < 1$ as otherwise in a single-step interfacial electrochemical ET. This is because the physical meaning of κ_i in eqs 3 and 4 is now different and represents electronic broadening of the molecular redox level from the interaction with the enclosing electrodes and, in this way, the number of electrons transferred. As a final note, $T_{\epsilon A}(\epsilon;\,\eta)$ in eq 4 refers to electronic coupling between the molecular redox level and individual electronic levels in the enclosing metallic electrodes. The individual $T_{\epsilon A}(\epsilon;\,\eta)$-values are infinitesimally small but appear in macroscopically large numbers roughly represented by the metallic electron densities and energy range in the combinations $\rho\kappa_{sm}k_BT$ and $\rho\kappa_{mt}k_BT$, eq 3. Overall the adiabatic tunneling current expression thus displays a formally similar strong dependence on the electronic coupling and a correspondingly strong (exponential) distance dependence as in one-electrode diabatic ET. The strong electronic coupling can, however, give much larger "apparent transmission coefficients" $\rho\kappa_i k_BT$ (>1), reflecting the different importance of this quantity in the two cases.

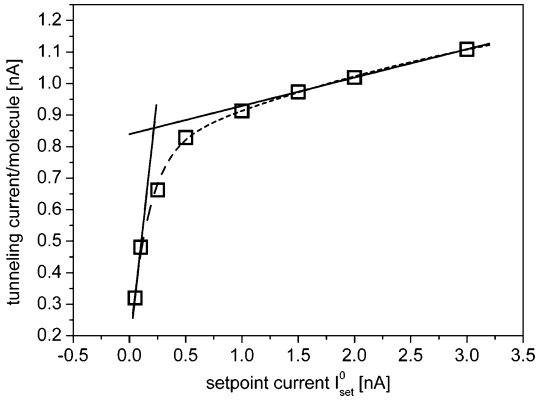

Figure 5. STS peak tunneling current/molecule as a function of setpoint current/distance for Osp0p on Pt(111), 0.1 M $NaClO_4$; $V_{bias} = -0.1$ V.

The data in Figure 5 illuminate the two-state tunneling mechanism in terms of the concepts and formalism in eqs 1−5. The peak currents, I_{tun}^{peak}, were determined from tunneling current/overpotential spectra at different setpoint currents, I_{set}°. These spectra were then fitted with a Gaussian, in order to determine their intensity.

Small setpoint currents correspond to large tip/molecule distances and (relatively) slow molecule/tip ET (small κ_{mt}), while large values of I_{set}° represent narrow tunneling gaps and (relatively) fast molecule/tip ET (large κ_{mt}). At sufficiently high I_{set}°/small tunneling distance, the STM tip will eventually contact the molecule and the substrate/molecule ET step will govern the overall tunneling current. This scenario is described by eq 5.

The total peak current also depends on both the tip quality and the molecular surface concentration. Blunt tips may result in more molecules participating in parallel in the conduction process. Different data sets were therefore first normalized to the number of participating molecules using the apparent current/molecule of 0.32 nA at $I_{set}^{\circ} = 0.05$ nA and $V_{bias} = -0.1$ V (Figure 4) and finally averaged (Figure 5).

The observed behavior accords with the physical picture described above. The change in the $I_{tun}^{peak}/I_{set}^{\circ}$ correlation over a narrow I_{set}° range corresponds to a transition from weak (small I_{set}°) to strong (large I_{set}°) molecule/tip interactions. As I_{set}° becomes large and the molecule/tip distance becomes very small, the tunneling current/molecule changes much less and almost reaches a plateau. This also follows from eq 3, as κ_{mt} goes from a value comparable to κ_{sm} at large I_{set}° (small distances) to a much smaller value at small I_{set}° (large distances).

The initial strong increase of I_{tun}^{peak} with I_{set}° is also consistent with our previous work, where we determined an apparent decay coefficient β from tunneling current/distance spectroscopy.[24] β was found to be strongly dependent on the substrate potential with $\beta = 0.89$ Å^{-1} for E_s far away from E° (high effective tunneling barrier) and $\beta = 0.46$ Å^{-1} for $E_s \approx E^{\circ}$ (low effective tunneling barrier).

Upon further decrease in the tip/substrate distance, other effects may set in. Examples include tip-induced alterations in the molecule/substrate orientation, in the potential distribution at the redox site (cf. ξ and γ in the formalism above), and in the reorganization energy λ, due to a displacement of counter ions and solvent molecules in the tunneling gap.

The notion of fast molecule/tip ET is implicit in the discussion above. This is related to the electrochemical environment. In

contrast to air or a vacuum, there are generally networks of solvent molecules between the tip and redox molecule which are much more efficient for ET than through-space interactions.[60] The absence of substantial contact resistance on the molecule/tip side can be rationalized in this way. A similar finding was reported recently by Smalley et al., who compared heterogeneous ET rates of surface-attached redox species with those of dissolved complexes (no covalent attachment to the surface). Rate constants were found to be equal within a factor of 10.[61]

These observations can be combined with the data in Figure 5 to estimate the number of electrons transmitted per molecule in a single charge-transfer event, i.e., n_{el}. The tunneling current/molecule increased by a factor of 2.7 from $I_{set}^{\circ} = 0.05$ nA to the crossing of the two regression lines, Figure 5, yielding an extrapolated maximum tunneling current of $I_t^{mol} \approx 0.9$ nA/molecule or a conductivity of 9 nS/molecule ($V_{bias} = -0.1$ V). From the discussion in the previous section, this value is likely to refer to the tunneling configuration with contact between the molecule and the tip, which we focus on below.

Based on eq 5, the product $n_{el}k_{sm} \approx 5.6 \times 10^9$ s^{-1} can be calculated from the limiting current in Figure 5, (0.32 nA/molecule · 2.7)/e. There is no obvious way to determine these two quantities independently. Following our observation that tunneling current enhancement closely correlates with the monolayer electrochemical rate constant, we can, however, tentatively set $k_{sm} = k_{ET,ec}$.[24] This was estimated above as 10^7-10^8 s^{-1} for Osp0p (0.1 M $NaClO_4$); cf. also Supporting Information p S2.

For $k_{sm} = k_{ET,ec}$, n_{el} then amounts to 60−600, corresponding to $\Delta\epsilon = eV_{bias}/n_{el} = 0.17$ to 1.7 meV. This value is indeed significantly lower than $k_BT = 26$ meV, pointing clearly to adiabatic behavior. Accordingly, the formal apparent transmission coefficient for interfacial electrochemical ET corresponding to this value would be $\rho\kappa_{sm}k_BT \approx 15-150 >> 1$, which is also in the adiabatic regime. A value >1 for the latter is meaningful only to the STM configuration.

This discussion illuminates the nature of the tunneling process but is still a crude approximation. The electrochemical rate constant is measured in the absence of the STM tip. The close proximity of the tip and the associated strong electric field can affect ET kinetics in various ways, for example, by changing the reorganization energy (cf. above) and/or the electronic coupling (tunneling barrier). Even minor alterations (decreases) in λ thus significantly change (raise) the ET rate constant. Interfacial electric fields are also strong (10^7-10^8 V/m) in the absence of the STM tip and comparable to the tip-induced field. It should also be noted that the driving force effect due to eV_{bias} has been disregarded here.

A more complex overall tunneling mechanism may, finally, have to be considered as electrochemical ET kinetics data of Osp0p, Osp2p, and Osp3p monolayers have left some controversy.[39−46,58] These data show *both* strong distance *and* solvent dependence. This is difficult to explain exclusively *either* within a simple diabatic or adiabatic ET model *or* within stochastic chemical rate theory. The observations can be rationalized if a gating process precedes the ET step. Such a scenario was found for tunneling through alkanedithiols or conjugated phenyl−ethynyl−benzene wires.[36−37] So far, the present tunneling data can, however, be understood without introducing an additional gating mode.

4. Conclusions

Following previous work, we have shown that the tunneling current through a single or a few molecules can be modulated efficiently by the presence of an accessible redox level. The modulation is detected both directly, by measuring the tunneling current at constant distance and tip/substrate bias, and indirectly, by apparent height changes in the in situ STM images. The experimental data accord well with a view based on two-state electron tunneling via the redox center as the dominating charge-transfer process. Electron transport is addressed within the limit of adiabatic ET which is supported by the data. This constraint can, however, be relaxed straightforwardly. In the adiabatic regime, the electron is first transferred to the redox level (substrate → redox level → tip ET sequence). This level then relaxes toward a new reduced-state equilibrium configuration. Before the latter is reached, however, the electron is transmitted to the tip, as ET in the adiabatic regime is fast compared to the environmental relaxation. The redox level then receives a second electron from the substrate, etc., and a (large) number of electrons, n_{el}, are transferred within the nuclear relaxation time, τ_{nuc}, i.e. in a single in situ STM electronic event.

The tunneling current peak intensities display a discrete distribution. This enables determining a current/molecule of ~0.9 nA/molecule at small tip/substrate distances corresponding to a conductivity of 9 nS/molecule ($V_{bias} = -0.1$ V). Together with an estimate of the substrate/molecule rate constant based on extensive electrochemical data, this result was used to determine n_{el} and the effective electronic transmission coefficient, $\rho\kappa k_BT$. Both were found to assume large values, in the range of 60−600 and 15−150, respectively. These values place the substrate/molecule ET process clearly in the adiabatic regime and offer a clue to the high tunneling currents observed.

Acknowledgment. Support from the Danish Research Council for Technology and Production Sciences, the IHP Training Network SUSANA (Contract: HPRN-CT-2002-00185), and a Marie-Curie postdoctoral Grant (T.A.) is acknowledged.

Supporting Information Available: STM images of Osp0p; Estimation of k_{ET} for Osp0p. This material is available free of charge via the Internet at http://pubs.acs.org.

JA066213R

(60) Jones, M. L.; Kurnikov, I. V.; Beratan, D. N. *J. Phys. Chem. A* **2002**, *106*, 2002−2006 and references therein.
(61) Smalley, J. F.; Newton, M. D.; Feldberg, S. W. *J. Electroanal. Chem.* **2006**, *589*, 1−6.